Shalata *et al. Human Genomics (2025) 19:21*
https://doi.org/10.1186/s40246-025-00723-y

Human Genomics

RESEARCH

Open Access

Sengers syndrome caused by biallelic TIMM29 variants and RNAi silencing in *Drosophila* orthologue recapitulates the human phenotype

Adel Shalata[1,2,3*], Ann Saada[4,5,6], Mohammed Mahroum[1], Yarin Hadid[1], Chaya Furman[1], Zaher Eldin Shalata[2], Robert J. Desnick[7], Avraham Lorber[3,8], Asaad Khoury[3,8], Adnan Higazi[9], Avraham Shaag[10], Varda Barash[11], Ronen Spiegel[3,12], Euvgeni Vlodavsky[3,13], Pierre Rustin[14], Shmuel Pietrokovski[15], Irena Manov[16], Dan Gieger[17], Galit Tal[3,18], Adi Salzberg[3] and Hanna Mandel[3,18,19*]

Abstract

Purpose Sengers-syndrome (S.S) is a genetic disorder characterized by congenital cataracts, hypertrophic cardiomyopathy, skeletal myopathy and lactic acidosis. All reported cases were genetically caused by biallelic mutations in the *AGK* gene. We herein report a pathogenic variant in *TIMM29* gene, encoding Tim29 protein, as a novel cause of S.S. Notably, AGK and Tim29 proteins are components of the TIM22 complex, which is responsible for importing carrier proteins into the inner mitochondrial membrane.

Method Clinical data of 17 consanguineous patients featuring S.S was obtained. Linkage analysis, and sequencing were used to map and identify the disease-causing gene. Tissues derived from the study participants and a *Drosophila melanogaster* model were used to evaluate the effects of *TIMM29* variant on S.S.

Results The patients presented with a severe phenotype of S.S, markedly elevated serum creatine-phosphokinase, combined mitochondrial-respiratory-chain-complexes deficiency, reduced pyruvate-dehydrogenase complex activity, and reduced adenine nucleotide translocator 1 protein.

Histopathological studies showed accumulation of abnormal mitochondria. Homozygosity mapping and gene sequencing revealed a biallelic variant in *TIMM29* NM_138358.4:c.514T > C NP_612367.1:p.(Trp172Arg). The knockdown of the *Drosophila TIMM29* orthologous gene (*CG14270*) recapitulated the phenotype and pathology observed in the studied cohort. We expand the clinical phenotype of S.S and provide substantial evidence supporting *TIMM29* as the second causal gene of a severe type of S.S, designated as S.S- *TIMM29*.

Conclusion The present study uncovers several biochemical differences between the two S.S types, including the hyperCPKemia being almost unique for S.S-*TIMM29* cohort, the different frequency of MMRCC and PDHc deficiencies among the two S.S types. We propose to designate the S.S associated with *TIMM29* homozygous variant as S.S-*TIMM29*.

Keywords Sengers syndrome, *TIMM29*, AGK, CK, RCC

*Correspondence:
Adel Shalata
adel.shalata@b-zion.org.il
Hanna Mandel
hmandel2637@gmail.com
Full list of author information is available at the end of the article

Introduction

Sengers syndrome (S.S) is an autosomal recessive mitochondrial disorder, characterized by hypertrophic cardiomyopathy, skeletal myopathy, congenital cataracts and lactic acidosis [1–5]. The clinical course of the disease can vary widely, ranging from a severe fatal form- leading to death within the third year of age in around 86% of cases- [6] to a more benign form that allows survival into adulthood [5, 7]. There is also an isolated form of congenital cataract [8].

A significant step in delineating the genetic defect underlying S.S was the identification of variants in the Acyl-glycerol kinase (*AGK)* by three research groups [4, 9, 10]. Since then, bi-allelic variants in the *AGK* have been found in most reported S.S cases (~40) [5, 6, 11, 12]. A decade ago, AGK was known as a mitochondrial transmembrane kinase that catalyzed the phosphorylation of monoacylglycerol and diacylglycerol into lysophosphatidic and phosphatidic acid, which play important roles as secondary messengers and regulators of mitochondrial ultrastructure [4]. However, the abnormal AGK's kinase activity could not explain the pathophysiology underlying the discovery of adenine nucleotide translocator 1 (ANT1) protein deficiency reported in many S.S patients [13, 14], including those in our cohort.

Mitochondria require more than 1000 nuclear-encoded proteins to function properly [15]. Evolutionary conserved translocation machineries are responsible for their specific mitochondrial sub-compartment delivery and integration into the outer membrane, intermembrane space, inner membrane, and matrix [15–17]. Mitochondrial inner membrane contains two translocase machineries: TIM23 and TIM22. TIM23 transports proteins that possess matrix-targeting N-terminal presequence, [18, 19], whereas TIM22 complex mediates the import of hydrophobic proteins, which are targeted by internal targeting signals into the inner membrane. Variants in genes encoding various subunits of these mitochondrial translocation machineries cause a growing list of mitochondrial diseases [20].

Compared to yeast, the human TIM22 machinery has been less characterized. In humans, TIM22 is a 440-kDa complex comprising at least six components: the hypothetical channel-forming protein Tim22, three small Tim proteins (Tim9, Tim10a and Tim10b), Tim 29 and acylglycerol kinase (AGK) [19]. In 2017, two research groups demonstrated that, apart from the AGK having a first primary function of being a kinase, it also has a second major function, which is it being an essential component of the TIM22 protein translocase complex in human mitochondria. It facilitates the import and assembly of mitochondrial inner membrane proteins, including ANT1 [19, 21, 22].This discovery explained ANT1 deficiency existing in S.S individuals harboring biallelic variants in the *AGK* [4, 5, 11, 13, 23]. Recently, biallelic variants in the *TIM22* pore forming subunit were identified and associated with hypotonia, gastroesophageal reflux and elevated lactate (CSF). Patient fibroblasts displayed reduced oxidative capacity, altered mitochondrial morphology and ANT1 deficiency [24]. Variants in the *TIMM8A* gene also called *DDP1* cause deafness dystonia syndrome [25].

This study focused on characterizing the clinical, biochemical and molecular mechanism underlying the pathogenicity of a homozygous missense variant identified in *TIMM29* (*C19orf52)* encoding Tim29 protein. Initially, the function of the gene was unclear, but it was later identified as a subunit of TIM22 [19, 21, 26, 27]. We demonstrated that the variant segregated in a cohort of 17 consanguineous individuals, who displayed the severe infantile form of S.S, but had no variant in the *AGK* gene. RNA interference (RNAi) was used to knock down or reduce the expression of the orthologue *of TIMM29* (*CG14270*) in *Drosophila*. The affected flies displayed characteristics similar to the human S.S infantile phenotype. This work has provided substantial evidence that *TIMM29* constitutes the second causal gene of S.S, which is herein designated as Sengers-syndrome type2 (S.S-*TIMM29*). This designation makes it different from the S.S caused by mutations in the AKG gene (S.S-*AGK*).

Research participants and methods

Participants

Over the past three decades, we have been conducting investigations involving 17 individuals from a large consanguineous Arab family (Table 1, Fig. 1). The clinical and biochemical phenotype of these participants resembled those seen in patients with fatal infantile S.S. We conducted a comprehensive study, including clinical, biochemical and genetic analyses in all the available individuals. Detailed description and methods can be found in the Human Genomics manuscript. It includes information on clinical phenotype, biochemical analysis, metabolic, and human molecular evaluations as well the methodology used for *Drosophila* Knock down experiments. Also included aredetailed description of mitochondrial isolation and respiratory chain complexes analyses in human and fly samples [28–31], linkage analysis, DNA sequencing (Sanger and Next Generation Sequencing-NGS), mitochondrial DNA analysis, Western Blot analysis**,** RNA expression analysis and transmission electron microscopy (TEM**)**.

Table 1 Clinical and biochemical characteristics of patients with Sengers syndrome-TIMM29

No in kindred	M or F	Age of diagnosis			"Routine" assays		Death m/d	Clinical remarks
		hypotonia	Cataract	CM m /d	Lactate pl/CSF	CK		
VI-8	F	2 m	s2m	4 m	8.2	NA	4 m	A few hours following cataract operation, she developed cardiorespiratory failure necessitating mechanical ventilation. Only then, CM was diagnosed. She died 2 days later with severe metabolic and lactic acidosis
VI-10	F	2nd d	–	–-	9.0	920	3d	Full term; Apgar 8/9; weight 3600gr; Age 2 h: apneic spells& cardiac arrest
VI-12	M	4 m	2 m	4 m	3.3	9469	11 m	The baby was diagnosed soon after birth due to previously affected siblings. He was severely hypotonic, and very alert. At age 8 month he sat unassisted
VI-14	F	3 m	3 m	3 m	NA	NA	4 m	Medical file not available. Cataract and CM were reported by the parents
VI-15	F	1st d	2 m	2 m	12.2	5,651	4 m	Early diagnosed due to previously affected sibling (case report VI-14, in supple)
VI-20	F	1st d	–	2 m	13/5	7800	3 m	She had no social eye contact (no cataract); elevated CSF lactate
VI-21	F	1st d	1d	2 m	24	3,122	5 m	Early diagnosis due to previous family history; had all S.S constituents;
VI-22	M	2nd d	2d	3 m	6.3/8.1	6,838	3 m	Presented at age 2d with tachypnea and lactic acidosis. CM was documented for the 1st time only one week prior to death at age 3 m'
VII-2	F	12 m	2 m	12 m	10	113	21 m	Had the longest longevity. Psychomotor development at age 13 m: very alert, severe hypotonia; could sit and stand unassisted, and walked with assistance. Spoke many wards with a faint voice
VII-3	M	1st d	–	–	7.8	2500	7 d	Premature; severe metabolic acidosis; died due to "neonatal sepsis"
VII-4	F	4 m	–	6 m	17.5	36,280	6 m	At age 4 m admitted for evaluation of FTT and absence of social eye contact, but no cataract. She had tachypnea, severe hypotonia and lactic acidosis. Markedly elevated serum CPK (rhabdomyolysis), with myoglobinuria. Mild C.M and poor left ventricle function recorded for the 1st time 4 h before death
VII-5	F	1st d	–	4 m	7.0/4.8	3600	5 m	Prematurity; Developmental delay and abnormal brain imaging (see supplements); Elevated CSF lactate; bilateral inguinal hernia;
VII-6	F	2 m	2 m	2 m	6.5	1933	2 m	Presented at age 2 months with all clinical constituents of seemingly S.S. She died 24 h after diagnosis of C.M of cardiorespiratory failure
VII-10	M	2d	–	2d	13.1/1.6	985	9d	Full term. Presented at age 24 h with hypotonia, cyanosis, and tachypnea necessitating mechanical ventilation. Echocardiography: sparkling of cardiac muscle. Elevated blood lactate 13.2, normal in CSF
VII-11	F	–	2 m	–	13.2	NA	4 m	There was no evidence of hypotonia nor cardiomyopathy prior to cataract extraction age 4 m'. "Crib death" was reported one week following operation
2009	F	1d	–	7d	12.8	4130	13d	Apgar 9/10; respiratory failure age 1d'; CM age 7d'; died age 13d;

CM-Cardiomyopathy; FTT-failure to thrive; Lactate mmol/l in Pl/CSF-Plasma/Cerebrospinal fluid; NA-not evaluated; m/d-months/days

Results

Clinical and laboratory evaluation

The family disease of the study participants was compatible with an autosomal recessive disease (Fig. 1).

All affected participants displayed a fatal mitochondrial disorder which strikingly resembled the infantile

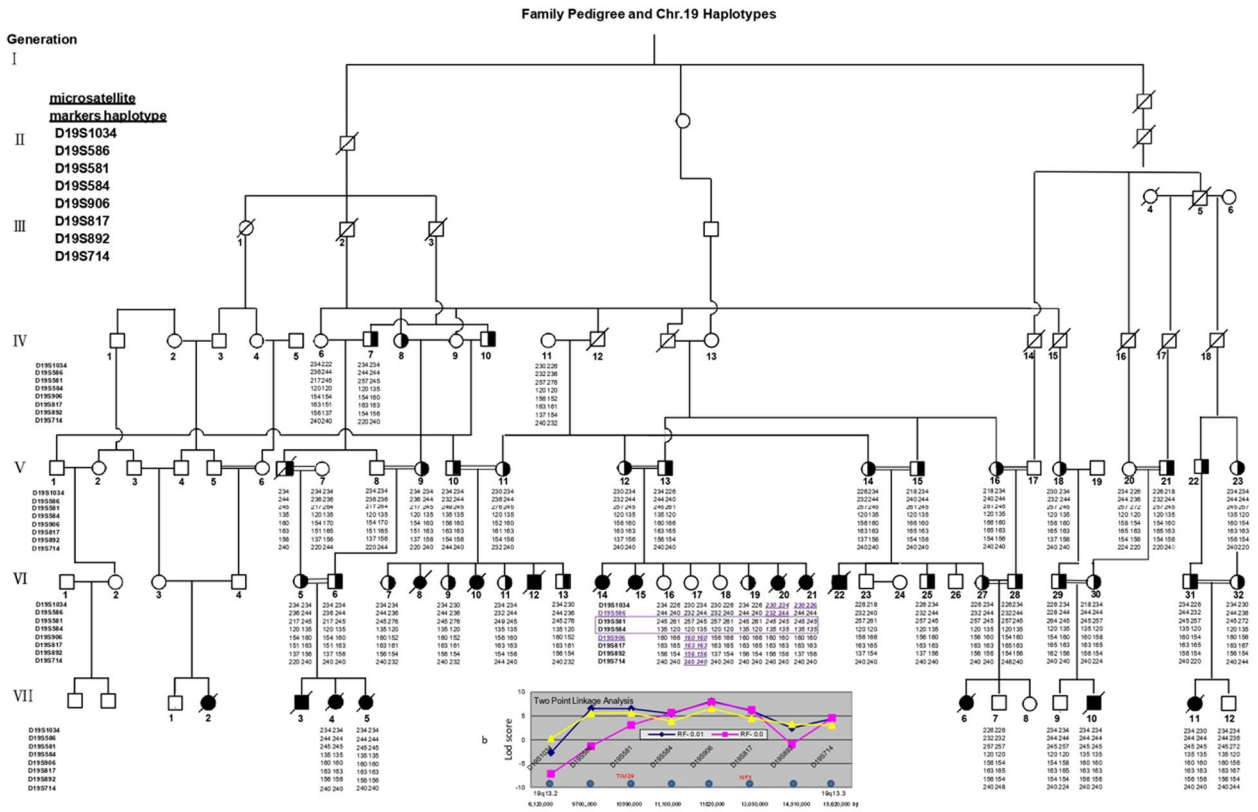

Fig. 1 The pedigree of the autosomal recessive *TIMM29*-Sengers syndrome family and localization of the disease-associated gene. Haplotypes of tested members of the 9 nuclear subfamilies. The originally linked region was further refined to a 2.3 Mb region with the use of recombination events detected in the nuclear subfamily [V-12&V13]. The pedigree includes the allele sizes of the microsatellite markers in the critical region on chromosome 19. Individuals whose DNA was available for analysis are annotated. The region of shared homozygosity is marked. The markers of the haplotype are listed in the column on the left side of the pedigree. The lower inset demonstrates the two-point linkage analysis as described by the Superlink (http://cbl-hap.cs.technion.ac.il/superlink-snp). The Lod score results (Y axis) of 8 microsatellite markers (depicted on the X axis) and their physical position are indicated according to the UCSC Genome Browser on Human Dec. 2013 (GRCh38/hg38) Assembly). Superlink was used to generate these results: Number of markers = 8; Mode of inheritance (MOI) = Recessive 0 0 0.99; Disease mutant gene frequency = 0.01. The family data file as well as the multipoint analysis can be found in the supplementary section

form of S.S. The clinical and biochemical features of the 17 individuals are depicted in Table 1. Typical clinical findings which are not depicted in the column of clinical remarks in Table 1 are provided in the case reports (Human Genomics). 16 out of the 17 studied participants displayed progressive hypotonia, while 8 out of them had hypotonia during the first two days of their life. Hypotonia was not found in participant VII-11, who suddenly died at the age of 4 months. Her death was described as"crib death". On follow-up, most of the participants had motor developmental delay and muscle weakness to various extents attributed to the progressive mitochondrial myopathy.

No dysmorphic features were apparent in the studied group. However, two patients (VII −3 and VII-5) had facial features that were attributed to prematurity. 10 participants displayed cataract. Among these 10, two were diagnosed with cataract at birth, while cataract was diagnosed in the remaining 8 before they reached the age of three months. We assume that the other 7 died before they developed cataract. Hypertrophic cardiomyopathy was diagnosed in 14 individuals among the studied group. Out of these14 individuals, 2 were diagnosed with hypertrophic cardiomyopathy during the first week of their life, while the remaining 12 were diagnosed with hypertrophic cardiomyopathy between the ages of 2–12 months. We speculate that the other 3 participants died before they developed cardiac abnormalities which could be depicted by echocardiography (EC). This hypothesis is illustrated in the case of participant VII-4, where an EC performed five days prior to her death was reported as "normal". However, four hours before her death, upon arrival at the emergency room (ER), she featured cyanosis and bradycardia. Subsequent EC performed revealed for the first time moderate cardiac hypertrophy with an almost motionless left ventricle.

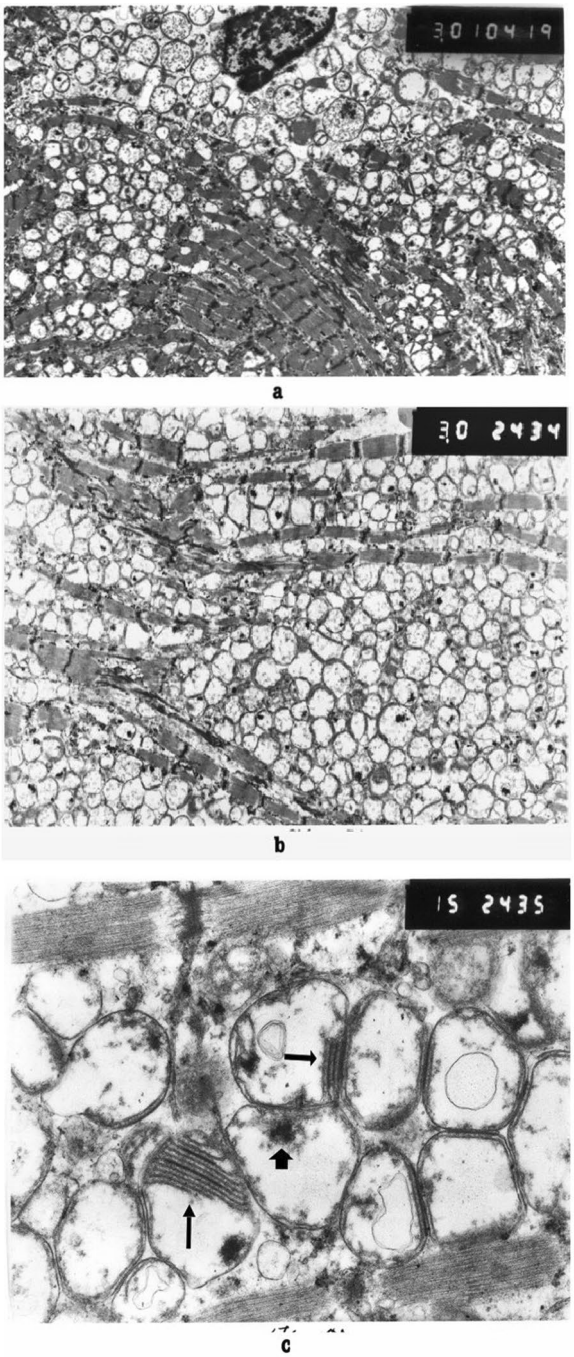

◀ **Fig. 2** a Low magnification. X3000, of ultrathin sections of muscle showing interrupted myofibrils with numerous, small and large abnormal looking electron lucent mitochondria ("mitochondriosis" or oncotic transformation of mitochondria). Most of the mitochondria lost their cristae; only few irregular and degenerated cristae are seen. **b** Higher magnification, X9000, showing isolated and disrupted myofibrils and replacement of heart muscle by proliferation of mitochondria mass. The mitochondria themselves show fluffy bodies and abnormal cristae which have been reported in other mitochondrial disorders. The massive proliferation of the mitochondria could be termed: "oncocytic" transformation or "mitochondriosis". **c** High magnification X15,000, showing a mass of abnormal mitochondria between isolate myofibrils. Most of the mitochondria lost their cristae; only few irregular and partially degenerated cristae are shown (arrows). In a few mitochondria paracrystalline inclusions are seen (arrow head)

Surprisingly, the electron microscopy (E.M) of her cardiac muscle revealed only a few left isolated disrupted myofibrils and most of the heart tissue was replaced by massive proliferation of abnormal shaped mitochondria. Most of these mitochondria are without cristae (Fig. 2a,b and c).

Participant VII-11 did not show signs of cardiomyopathy on Echocardiography (EC) in at the age of 4 months. She died at home two weeks later, during sleep at night. We assume that her "sudden death" may have been caused by cardiac arrhythmia. This is similar to the case of a two-year-old patient that died suddenly of cardiorespiratory arrest, even though he had stable cardiac function 1 month prior to his death [11]. 15 of the studied participants died before reaching the age of one year. 4 of them died in the neonatal period; only 2 of them, who seemed to have a somewhat milder phenotype, survived until the age of 21 months (Fig. 1 and Table 1-VII-2).

All participants had elevated plasma lactate level which fluctuated between 2.9 and 17.5 (normal up to 2 mmol/l). Lactate level was elevated in the cerebrospinal fluid (CSF) of two out of three participants (VI-10 and VII-5) who underwent lumbar puncture, which is suggestive of the involvement of the central nervous system (CNS). Serum alanine, which is known as a marker of inborn errors of energy metabolism [14], was elevated in most of the studied participants.

Most of the routine and metabolic laboratory studies (see in the methods section) were found to be within normal ranges. However, remarkably, 13 out of 14 studied participants had elevated serum creatine phosphokinase (CK) levels greater than 1000 U/L (hyperCKemia), in the range compatible with rhabdomyolysis [32]. HyperCKemia has not been reported nor considered as a common marker in previously reported S.S-AGK cases. Recently, only one S.S-*AGK* reported case featured elevated CK and myoglobinuria [12].

Urinary organic acids of eight patients were studied. The results showed that the patients exhibited different urinary organic acids profiles, ranging from normal to intermittently increased secretion of various metabolites commonly secreted by patients with mitochondrial disorders. They included lactate, succinic acid, fumarate and 3-hydroxyglutaric, suggesting the involvement of the Kreb's cycle, 3- hydroxybutyrate (ketosis) and

occasionally 3-methylglutaconic acid, known to constitute a non-specific marker for various mitochondrial disorders [33]. It is worth noting that we did not identify a constant and pathognomonic abnormal profile, for the SS-*TIM29* mitochondrial disorder.

Histology and histopathology of skeletal and cardiac muscle specimens

Seven of the studied participants were subjected to histopathological analyses. Skeletal muscle biopsy specimens from 4 of them were subjected to histopathological analysis using light microscopy. While, histopathological analysis was performed on the cardiac muscle of the remaining three, using standard techniques. Light microscopy revealed minimal to significant variation in fiber size and increased glycogen and lipid droplets to various extents. We used specific stains for COX and succinate dehydrogenase (SDH). They revealed some of the participants had COX deficient fibers, increased SDH staining and ragged red fibers commonly reported in patients with mitochondrial myopathy.

The electron microscopy (EM) study of skeletal muscle and myocardial-biopsy specimens, performed within 1–2 h after the biopsy or post mortem, revealed interrupted myofibrils with numerous electron lucent mitochondria. Higher magnification shows isolated disrupted myofibril and replacement of heart muscle by marked proliferation namely, oncocytic transformation of abnormal looking mitochondria of various sizes and shapes (Fig. 2a,b and c). Such mitochondrial ultrastructural changes are not pathognomonic for S.S-*AGK* nor for S.S-*TIMM29* since it has been found in other mitochondrial disorders [3, 34–36].

Mitochondrial respiratory-chain complexes activities

Over the years, muscle biopsies have been performed in most of the S.S-*TIMM29* participants, in which the activities of respiratory chain complexes were assessed. Table 2 provides the results obtained from the study of respiratory chain complexes activities, citrate synthase (CS) and pyruvate dehydrogenase complex (PDHc) activities examined in mitochondria extracted from 4 fresh skeletal muscles and one frozen cardiac muscle. We demonstrate various combinations and extents of decreased mitochondrial respiratory-chain-complex activities in the participants. A similar pattern was demonstrated in a frozen cardiac muscle specimen. Fibroblast culture retrieved from one participant (VII-3) revealed only a mild defect in the mitochondrial function with an increased CS activity. This finding might denote that cultured fibroblast does not constitute the ideal tissue for studying the effect of Timm29 deficiency. Generally, complex II activity (composed solely of nuclear encoded proteins, without mitochondrial DNA (mtDNA) encoded proteins) ranged between low or slightly below normal to increased levels. Pyruvate dehydrogenase complex (PDHc) deficiency was also demonstrated in 4 of the studied participants (Table 2).

Linkage analysis and positional cloning

In our previous study on homozygosity mapping and positional cloning on participants VI-20, VII-4, VII-10 and VII-11 (Fig. 1) utilizing the DNA pooling strategy [37, 38], we localized the disease gene locus to 19p13.2–3 chromosomal region of 2.3 Mb interval between the markers D19S586 and D19S906 (LOD score of 7.89 for two-point linkage analysis for marker D19S906 (Fig. 1) and of 12.38, $\Theta = 0$ for multipoint linkage analyses for the markers D19S584, D19S906 and D19S817). For LOD score calculation, we used the Superlink software (http://cbl-hap.cs.technion.ac.il/superlink-snp) [39].

TIMM29 mutated in S.S type2 individuals

We performed direct Sanger sequencing of 14 out of 84 genes located between the D19S586 and D19S906 markers (19p13.2–3; UCSC Genome Browser on Human Mar. 2006(NCBI36/hg18)), selected by their high scores as mitochondrial encoding proteins according to predicting tools (e.g.MitoPROT2, Mitopred, Predotar and TargetP). The sequences of all the genes were normal except one missense point variant (NM_138358.4:c.514T > C NP_612367.1:p.(Trp172Arg) in *C19ORF52* (*LOC90580*) gene which was renamed as *TIMM29* [19]. In genomic level, this variant is known as NC_000019.9:g.11040109T > C NM_138358.4:c.514T > C p.(Trp172Arg) (Fig. 3a). This variant was tested in 4 of our studied affected participants and in 51 healthy parents and siblings. The variant segregated with the disease and matched the haplotype carrier status, as described in Fig. 1. Thus, all affected individuals were homozygous for the c.514T > C variant. While the parents were heterozygous, the siblings and additional healthy family members were either heterozygous or homozygous for the wild allele (c.514T). Also, this variant was not present in 200 chromosomes from 100 unaffected, unrelated healthy individuals from the same ethnic background. A new SS-*TIMM29* affected neonates were born in 2009 and 2024 (Table 1). The parents of both patients were 3rd degree cousins and belong to the expanded affected family. The patient 2009 was homozygous for the disease haplotype (data not shown) and her phenotype was extremely severe and she died at age 13 days of life. While, the patient HZ 2024 was 5 months old in his last examination. Both were homozygous and the parents were heterozygous for the *TIMM29* NM_138358.4:c.514T > C.

Table 2 enzymatic activities of the mitochondrial respiratory chain and mtDNA quantitation in mitochondria from fresh muscle, frozen myocard and fibroblasts

Patient in pedigree		**VII-4**	**VII-2**	**VII-5**	**VII-11**		**VII-12**		**VII-3**
Age	**Normal range ± SD**	**5d**	**1y**	**4 m**	**4 m**	**Normal**		**Normal range ± SD**	
Specimen	**Fresh muscle n = 20**	**Fresh muscle mitochondria**	**Fresh muscle mitochondria**	**Fresh muscle mitochondria**	**Fresh muscle mitochondria**	**Frozen myocard n = 2**	**Frozen myocard mitochondria**	**Fibroblast n = 10**	**Fibroblast mitochondria**
Assay (nmol/min/mg)									
Citrate synthase	2120 ± 370	1380	3200	4400	3160	1470	4350	249 ± 97	388
NADH-ferricyanide reductase (C I)	4650 ± 102	1700 (56%)	1400 (20%)	2560 (27%)	1700 (25%)	4900	3400 (23%)	nd	nd
NADH-CoQ reductase (C I)	274 ± 127	nd	nd	21 (4%)	92 (23%)	nd	nd	31 ± 11	33 (61%)
NADH-cytochrome C- reductase (C I + III)	508 ± 164	109 (59%)	113 (15%)	36 (6%)	248 (33%)	180	37 (7%)	nd	Nd
Succinate-cytochrome C- reductase (C II + III)	340 ± 84	131 (27%)	126 (25%)	120 (17%)	188 (37%)	135	124 (30%)	131 ± 44	138 (64%)
Succinate-CoQ reductase (C II)	77 ± 15	62 (123%)	67 (57%)	108 (67%)	106 (92%)	147	124 (29%)	nd	Nd
Succinate dehydrogenase (CII)	327 ± 52	188 (88%)	245 (49%)	455 (67%)	352 (72%)	110	354 (108%)	68 ± 31	78 (72%)
Ubiquinol-cytochrome C-reductase (CIII)	4270 ± 97	1120 (40%)	1440 (22%)	900 (10%)	2000 (31%)	nd	nd	nd	Nd
Cytochrome c oxidase (CIV)	1346 ± 327	272 (30%)	328 (16%)	216 (7%)	285 (14%)	1145	775 (16%)	412 ± 59	646 (94%)
Mg ATP:ase V	721 ± 203	90 (19%)	165 (15%)	49 (3%)	104 (10%)	194	10 (2%)		
Pyruvate dehydrogenase complex	80 ± 24	10 (19%)	15 (13%)	0.8 (10%)	8.3 (7%)	57	44 (26%)		
Pyruvate + malate oxidation	127 ± 27	nd	23 (12%)	10 (4%)	17 (9%)				
Glutamate + malate oxidation	151 ± 54	nd	18 (8%)	13 (4%)	21 (9%)				
Succinate oxidation	169 ± 41	nd	41 (16%)	38 (11%)	35 (14%)				
Ascorbate + TMPD oxidation	375 ± 108	nd	139 (25%)	85 (11%)	129 (23%)				

Mitochondrial enriched fraction isolated from muscle tissue was studied in all patients. The activity of citrate synthase is expressed as a percentage of the control mean (2.12 µmol/min /min mg protein). The activity of all other enzymes is given as a percentage of the mean, normalized for citrate synthase activity. nd = not determined. (%) percentage of control value normalized to citrate synthase

With the emergence of Next Generation Sequencing (NGS) technology, in order to cover all genes including those located in 19p13.2–3 mapped region (Human Genomics), we ran Exome Sequence (ES) analysis in the different participants using two different platforms six years apart and reanlyzed the last ES few months ago. In the first round, ES was performed in one nuclear family (patients VII-3 and VII-4 and parents VI-5, VI-6, Fig. 1) and the analysis did not reveal any pathogenic or likely pathogenic variant. NC_000019.9:g.11040109T > C NM_138358.4:c.514T > C p.(Trp172Arg) variant was not detected. To explain this, we focused on the 944 exons located within 19p13.2–3 disease refined mapped region. In conclusion, the coverage was not optimal since, only

605 exons (0.6408) were completely sequenced, while for the 339 remaining exons, the sequence coverage was incomplete. In 71 exons (0.075), over 80% of the exons' length were covered and sequenced, in 73 exons (0.077), 50–80% of the exons' length were covered and sequenced, in 92 exons (0.097) less than 50% of the exons' length were covered and sequenced and 103 exons (0.109) were entirely uncovered. Moreover, we zoomed in *TIMM29* gene by the Integrative Genome Viewer (IGV) and found a small region within exon 2 of *TIMM29* that was entirely uncovered, including the NC_000019.9:g.11040109T and flanking sequence.

Six years later, we ran ES in patient VII-10 (Fig. 1) by using Nextera DNA Flex Enrichment reagents and NovaSeq 6000 sequencer (Illumina, San Diego, CA). The coverage and depth were obviously much higher (pptx VII-10 Human Genomics) and the analysis identified the *TIMM29*, NM_138358.4:c.514T > C NP_612367.1:p.(Trp172Arg) variant in homozygous state. Importantly, no other pathogenic or likely pathogenic variants were found. Of note, there was no evidence for nuclear copy number variation (CNV), mitochondrial genome point variants and deletions. Reanalysis of ES raw data performed 4 years later for patient VII-10 did not change our primary finding (Human Genomics).

At the genomic level, *TIMM29* is composed of 1494 base pairs and has two exons separated by 83 base pairs intron. The 1394 nucleotide mRNA encodes for a 260 amino acids protein of 29.233 kDa molecular weight. *TIMM29* has no splice isoforms. *TIMM29* is a ubiquitously gene with abundant orthologues present across a wide range of species, including mammalian, amphibian, avian, fish, vertebrates, sea urchin (Strongylocentrotus purpuratus), phylum Placozoa (Trichoplax adhaerens), *Drosophila* and *c. elegans.* For sea urchin, phylum Placozoa, *Drosophila* and *c. elegans*, it has 40%, 29%, 28, and 25% conservation over the length of the protein, respectively. At the protein level, Tim29 Trp172 residue is highly conserved in evolution (Fig. 8a) [19, 26]. It is almost fully buried within the TIM22 complex structure facing the inner membrane, and only directly interacts with other Tim29 residues [22] (Fig. 8b). A blast search analysis revealed that Tim29 protein shares high amino acid homology that ranges from 35% up to 98% with proteins from various species. The analysis and a multiple sequence alignment also revealed a high protein similarity among Tim29 orthologues across diverse species. Of note, as the Trp172Arg variant is a change that is not observed in any orthologue (Fig. 3a, b and 8a), the p.Trp172Arg variant results in the substitution of the hydrophobic aromatic side chain tryptophan for the positively charged side chain arginine at position 172 of the Tim29 protein [19]. 14 prediction tools considered this variant as "pathogenic", while five others considered it as "benign" (Human Genomics xls2) selectively. Here, we mention c. 514T > C variant scores in parentheses as they appear in different prediction tools, such as CADD (32.0); REVEL(0.646); phyloP(6.25) and PolyPhen(0.964). This supports the pathogenicity of this variant. Also, according to the gnomAD v4.10 (GRCh38) database, only three heterozygous variants in *TIMM29* gene (ENSG00000142444.7) p.Trp172 codon were described. The NC_000019.9:10929433T > C (chr19-10929433-T-C) (c. 514T > C) variant found in this study was reported to be heterozygous in only one individual of Middle Eastern origin with an allele frequency of 0.0001650. Moreover, NC_000019.9: 10929434G > A chr19-10929434-G-A (p.Trp172Ter) variant (rs778791266) was reported heterozygous in two individuals of European non-Finnish origin. The NC_000019.9: 10929434G > T (chr19-10929434-G-T) variant was reported to be heterozygous in three individuals (one of South Asian origin

(See figure on next page.)

Fig. 3 **a** Chromatograms showing the *TIMM29* homozygous T > C transition found in patient sequences (VII-4 and VII-5), resulting in a missense variant in codon 172 where tryptophan was substituted for arginine (Trp172Arg). **b** The Tim29 Trp172 and neighboring amino residue orthologues ClustalW2 results. The Tim29 Trp172 is a highly conserved residue among species. **c** ClustalW2 aligment results of Tim29 human pW172 (Tryptophan) with 16 *Drosophila* species Tim29 Trp172 amino residue orthologues is replaced by a Tyrosine (Y) in most *Drosophila* species, including *Drosophila melanogaster*, and by a Phenylalanine (F) in certain species such as *Drosophila persimilis.* **d** Western blot was performed with mitochondrial(lanes a1 and b1)and intermyofibrillar homogenate (lanes a2 and b2), extracted proteins from two musculoskeletal samples of two healthy controls a and b. The blotted membrane was then exposed to anti Tim29 Ab, 1:400 dilution. The Tim29 protein was purely transported to the mitochondria and was not detected in the intermyofibrillar homogenate. **e** Mitochondria were isolated from quadriceps 1–3 and heart 4–6 from controls 1 and 4 and patients 2,3,5,6 (patients: VII-4 and VII-5, respectively). The proteins were separated by SDS-PAGE (CII, AIF, TIM29) or urea-PAGE (CIV Subunit 2) and subjected to western blot analysis. Compared to control group, the TIM29 was decreased (muscle) or barely detectable (heart) in the patient group. ANT1 was undetectable in patient VII-4 (Western blot performed in a separate gel). **f** There is a decrease in two constituents of cytochrome C oxidase (complex IV) in both COX II, which is a mitochondrial encoded protein and in subunit IV, which is encoded by the nuclear genome. There is severe deficiency of ANT1. Regretfully, we only had a very limited amount of patient material and nothing was left after analysis, so we cannot repeat the blots. However the lanes were loaded with the same amount of the citrate synthase units, equivalent to 2.5 mU per lane. Thus, we relate to citrate synthase as a proper loading control that is not predicted to be affected by the *TIMM29* variant. P = patient (represent all tested patients (14); C = Control

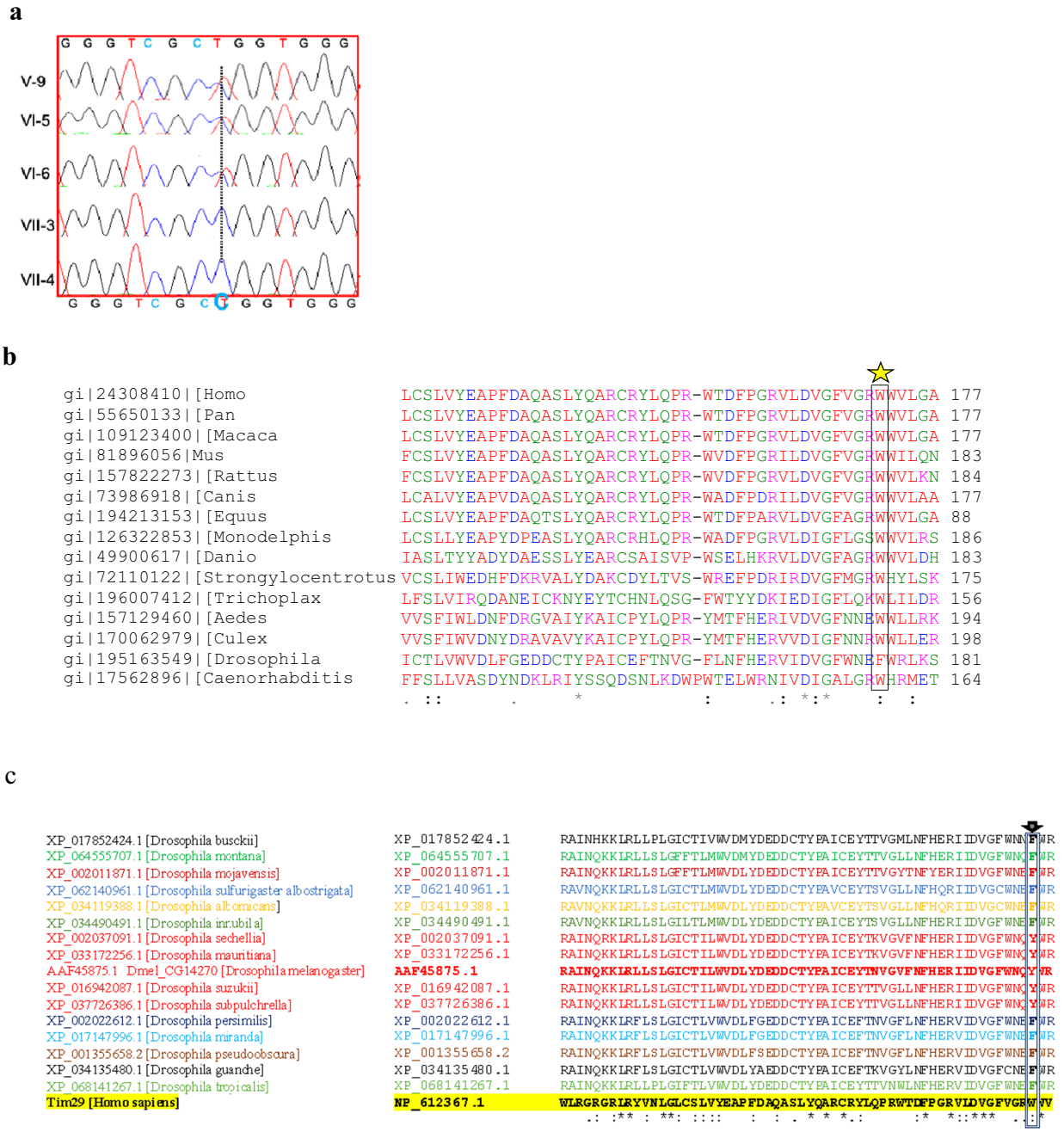

Fig. 3 (See legend on previous page.)

and remaining two unspecified). Finally, NC_000019.9: 10929435G > A (chr19-10929435-G-A) variant was reported to be heterozygous in one individual of European non-Finnish origin. The termination variants were predicted to be pLoF with high-confidence. pTrp172Leu variant was predicted to be probably-damaging in Polyphen and damagaing in SIFT.

From the information obtained from the databases (gnomAD, ClinVar, ExAC), we can say that *TIMM29* variants appear in low allele frequency. From gnomAD v4.10 (GRCh38), there are 734 variants (61 LoF, 454 missense and 219 synonymous) in *TIMM29* gene. All of the LoF and missense variants were reported in heterozygous state only. Also, repeated GeneMatcher searches were negative.

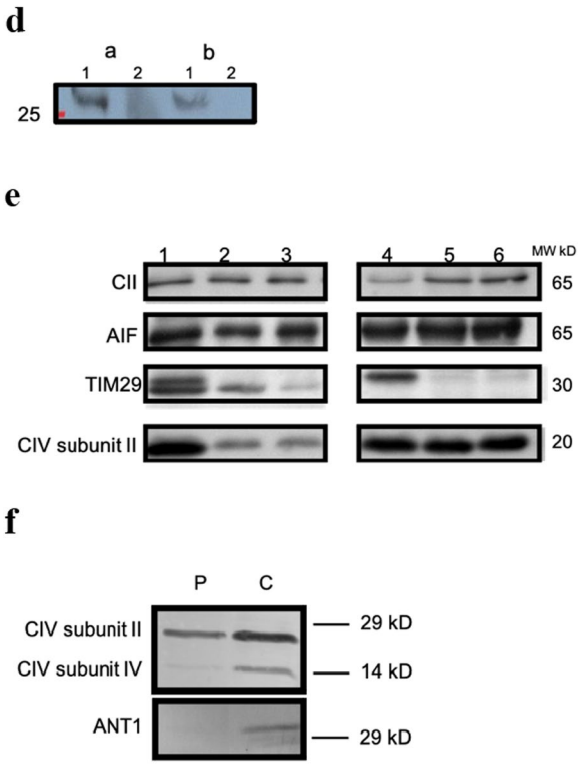

Fig. 3 continued

Tim29, ANT1 and OXPHOS protein levels

We studied the impact of ^{172R}Tim29 variant on the protein level of Tim29 itself and on several other mitochondrial proteins, using available skeletal-muscle biopsy specimens and primary fibroblasts cultures. It was done to show that *TIMM29* variant is linked to S.S-*TIMM29*. Western blot analysis showed markedly reduced Tim29 levels along with reduced levels of ANT1 and other OXPHOS proteins (Fig. 3b, c, d, e ,f). These findings support the notion that the ^{172R}Tim29 variant adversely affects the stability of the Tim29 protein, ANT1 and several OXPHOS proteins encoded by both the mitochondrial and the nuclear genomes. The decreased levels seen in the various OXPHOS proteins in tissues with Tim29 deficiency show that Tim29 plays an essential role in the TIM22 complex [19, 26].

Mitochondrial DNA content and transcription

In all the studied participants described above, the function of the respiratory complexes I, III, IV, and V was disrupted, while the function of complex II, solely composed of nuclear encoded proteins was elevated, within normal range or slightly reduced. Thus, we examined mtDNA content in the studied participants, which was found to be normal or elevated (results not shown). In addition, we sequenced the entire mtDNA (coding genes, mitochondrial tRNA and rRNA genes) excluding pathogenic mtDNA variants, depletion and mtDNA translation defects.

In order to assess the effect of mtDNA transcription on the studied participants, we tested mitochondrial respiratory chain complexes representative genes, such as ND1 and ND2 for complex-I and ATP6 for complex V and detected normal or elevated levels. In addition, we tested two nuclear genes, *SLC25A4* (*ANT1*) and *TIMM29*. The expression analysis determined a normal mtDNA transcription level (Fig. 4 and, Table 2 and xls3 in Human Genomics). This demonstrates there is a normal *SLC25A4* mRNA expression, but markedly increased level (by more than five folds) of *TIMM29* mRNA expression in our S.S-Tim29 participants compared to the healthy control samples (Table 2 in Human Genomics, Fig. 4). Thus, according to our results, Tim29 deficiency does not affect transcription negatively.

Animal model

The knock down of CG14270 the Drosophila melanogaster TIMM29 orthologue

To further confirm the role of *TIMM29* as the causative agent of S.S type 2 phenotype, we examined the loss-of-function phenotype of the *Drosophila melanogaster*

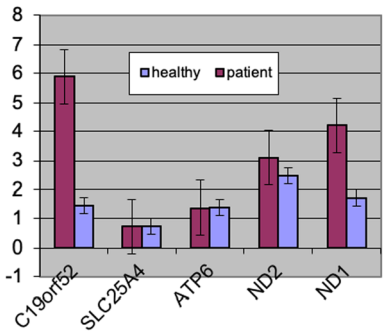

Fig. 4 representative musculoskeletal nuclear and mitochondrial gene expression. We used musculoskeletal samples from four controls and three S.S *TIMM29* patients for mRNA extraction. In order to compare the gene expression in the healthy and affected groups we used independent sample t-test. The expression data in S-Table 2 are the mean results of raw data. Apart from the *TIMM29* gene, there were no significant differences in the gene expression level between healthy and affected groups in the tested genes (*NDI, ND2, ATP6 & SLC25A4*). The *TIMM29* gene expression was more than five folds higher in the affected than in the healthy group (p value 0.005)

orthologue *of TIMM29*. The fly genome contains a single gene, *CG14270*, of the Tim29 protein family that shows a significant sequence similarity to Tim29 throughout its entire length [40]. To test for possible involvement of the *CG14270* gene in mitochondrial biogenesis or function, we knocked down its expression using RNA interference (RNAi) and examined the effects on the fly's locomotion and general behavior. We used the mesodermal driver *24B-Gal4* to drive the expression of two independent *CG14270*-specific RNAi transgenes (*P{kk100018}v107710* and *P{GD8280}v17459*) in mesodermal tissues, both of these RNAi constructs have zero off targets [41]. Testing the effect of *P{kk100018}v107710* on *CG14270* epression by QRT-PCR, demonstrated a 6.6 fold decrease in expression in *P{kk100018}v107710/+;24B-gal4/+* larvae as compared to control *P{kk100018}v107710* larvae (Fig. 5E). Driving *P{GD8280}v17459* expression caused embryonic or larval lethality (in all temperatures tested from 18° to 29°). The expression of *P{kk100018}v107710* caused semi-lethality. Approximately 50% of *P{kk100018}v107710/+;24B-gal4/+* flies died as pharate adults (113/223). Some of the flies had difficulties eclosing from their pupal case and they died while trying to eclose (Fig. 5A). The progeny that did emerge appeared very lethargic, they did not eat and displayed dramatic reduction in climbing activity from day 1 of life (Fig. 5B–D, and video MVI-1 in Human Genomics). Whereas 83.5 ± 15% of control flies climbed from the bottom of the vial to a 5 cm height within 10 s or less (n = 49) after being knocked down to the bottom of the vial, none of the knockdown flies reached the 5 cm line within 10 s (n = 87).

The *P{kk100018}v107710/+;24B-gal4/+* flies started to die within a day or two post eclosion and did not survive more than six days, compared to the control flies that survived for several weeks.

The dramatic behavioral phenotypes caused by reduction in *CG14270* expression led us to examine directly the mitochondrial phenotype in the flight muscles of *CG14270* knocked-down flies, using transmission electron microscopy. The EM analysis showed substantial mitochondrial phenotype (Fig. 6), resembling the phenotype seen in muscle biopsies from S.S patients (Fig. 2). The mitochondria of the indirect flight muscles appeared swollen and presented extensive vacuolization of the inner membrane (Fig. 6). Disorganized musculature led to the progression of mitochondrial pathology. We could see a largely increased number and reduced size of mitochondria conforming with mitochondrial oncocytic.

Encouraged by the mitochondrial phenotype observed by EM in the indirect flight muscles of the *CG14270* knock-down flies, we studied the respiratory chain enzymatic activities assayed by spectrophotometry in muscle homogenates from the *CG14270* knockdown flies compared to normal flies. As presented in Fig. 7 and xls4 in Human Genomics, there was a significant decrease in the respiratory chain enzymatic activities in the RNAi treated flies compared to the control group. Altogether, the *CG14270* knock-down flies recapitulated the clinical and biochemical phenotype of S.S-*TIMM29*, type 2, which strongly provides evidence of the central role that *TIMM29* plays in causing S.S-*TIMM29*.

Discussion

Till date, all reported cases of S.S have been shown to be associated with homozygous or compound heterozygous variants in the *AGK* gene encoding the AGK protein (S.S-*AGK*) [4–6, 12]. We herein describe the results of the clinical, biochemical, molecular and functional studies in a cohort of participants who featured S.S phenotype, but had normal *AGK* gene sequence. Homozygosity mapping in this cohort located the disease gene in a 2.3 Mb interval on chromosome 19p13.2–3. A missense variant, NM_138358.4:c.514T > C NP_612367.1:p.(Trp172Arg) in *TIMM29* segregated completely with the disease (Fig. 1, xls1 in Human Genomics).

The various experimental validations, including in vitro analysis of tissues from the S.S- *TIMM29* participants and the use of a *Drosophila* model that recapitulated the human S.S-*TIMM29* phenotype provide strong substantiation for the pathogenicity of NM_138358.4:c.514T > C NP_612367.1:p.(Trp172Arg) variant in the *TIMM29* as the causal gene of S.S-*TIMM29* mitochondrial disorder. The protein level of Tim29 was significantly decreased in the participants' tissues (Fig. 3), even though

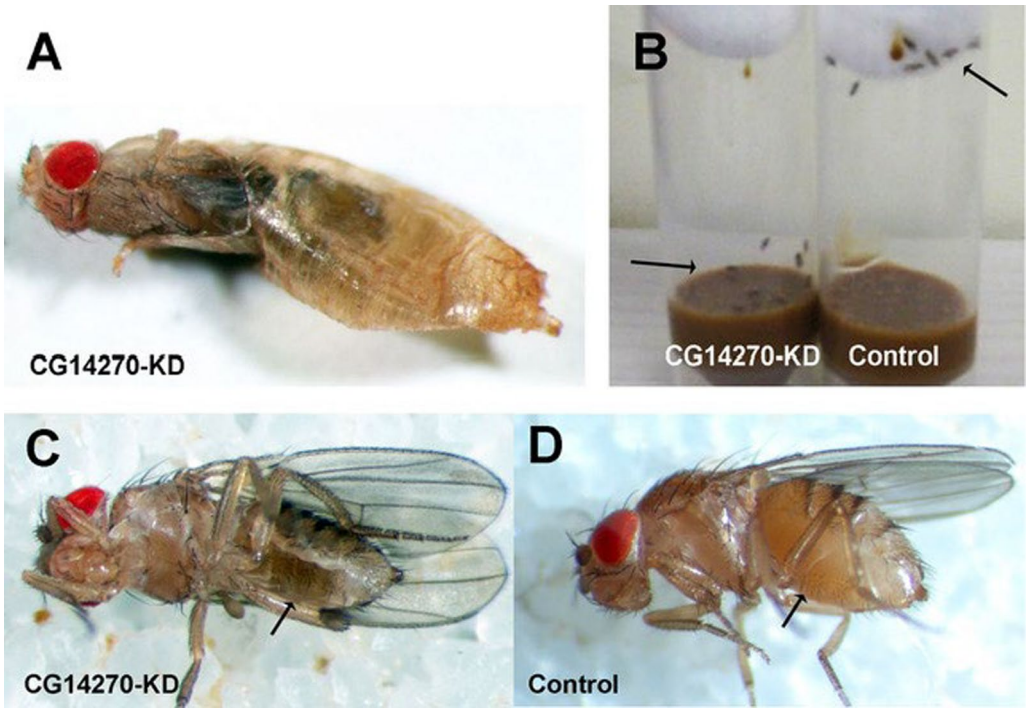

Fig. 5 Knocking down the *TIMM29* orthologue *CG14270* in mesodermal tissues leads to S.S-TIMM−*29*-like phenotypes. **A** A 107710kk/ + ;24B-gal4/ + (CG14270-KD) fly unable to eclose from the pupal case. **B** 107710kk/ + ;24B-gal4/ + flies that do eclose show extremely reduced motor activity and they fail to climb up the vial wall. The vial on the left contains 107710kk/ + ;24B-gal4/ + flies, and the vial on the right, control flies (arrows point to the position of flies). The flies in both vials were knocked down to the vial bottom and the picture was taken 30 s later (**C**–**D**). Heliyon video shows the locomotion activity of these flies. Surviving 107710kk/ + ;24B-gal4/ + flies do not eat as evident by their shrunken abdomen (arrow) (c) compared to control flies (**D**). **E** QFPCR amplification plot analysis in *Drosophila melanogaster* larva. Gene expression of two housekeeping genes, GAPDH and SDHA, was used as control. In both genes the expression results were similar and here we present the GAPDH data. For *GC14270* gene expression, we used two sets of primers (EX_PR_1 and EX_PR_2) located within the *GC14270* exon sequence. Here, we present the *GC14270* expression in *GC14270*- RNAi expressing larvae *(*107710kk/ + ;24B-gal4/ +) (lower plot) and control larvae (107710kk/ +) (upper plots) groups. The *GC14270* average expression in the RNAi-expressing larvae was reduced 6.6 folds (0.15) compared to the gene's expression in the control group (1)

TIMM29 mRNA expression increased by almost fivefold (Fig. 4 and Table 2 in Human Genomics). A similar finding was reported in a patient with compound heterozygous variants in *TIMM22* [24]. The increased mRNA levels of both *TIMM29* and *TIMM22* in the affected participants could result from an up-regulation of gene expression, a plausible hint for a common positive feedback regulatory system for TIM22 complex. The evolutionary conservation of the mutated Trp172 (Figs. 3; 8a), its replacement by the radically different Arginine residue, and its position and interactions within the TIM22 complex [22] (Fig. 8b) strongly suggest that the variant is highly deleterious. Indeed, we found that the*TIMM29* homozygous variant destabilizes Tim29 protein and leads to its degradation, as seen in the muscle specimens of S.S-*TIMM29* patients (Fig. 3). Consequently, Tim29 diminution in TIM22 complex is likely responsible for the severe phenotype of S.S-*TIMM29* mitochondrial disorder. Of note, Tim29 Trp172 is not conserved in *CG14270* (the *DrosophilaTIMM29* orthologue), and it was replaced either by Tyrosine (Y), in most *Drosophila* species, including *Drosophila melanogaster*, or by a Phenylalanine (F) in other species such as *Drosophila persimilis* (Fig. 3b, c). Since W, Y and F are all nonpolar aromatic amino acid residues that have hydrophobic side chain, we assume that this replacement keeps Tim29 activity intact. Although uncommon, there are known examples for a replacement of conserved tryptophan residues by phenylalanine in functional protein domains. For instance, in 33 rice Aux/IAA proteins, a conserved tryptophan residue, which is located in the central position of the functional protein domain IV was found in 31 proteins. It was replaced by phenylalanine in the 2 remaining proteins, without affecting protein activity [42].

Remarkably, the knockdown of *CG14270*, the *Drosophila TIMM29* orthologue, by RNA interference (RNAi) led to the recapitulation of the clinical, biochemical and histopathological phenotype of the human S.S-*TIMM29* participants. The knock-down flies exhibited the major constituents of the mitochondrial cytopathy exhibited

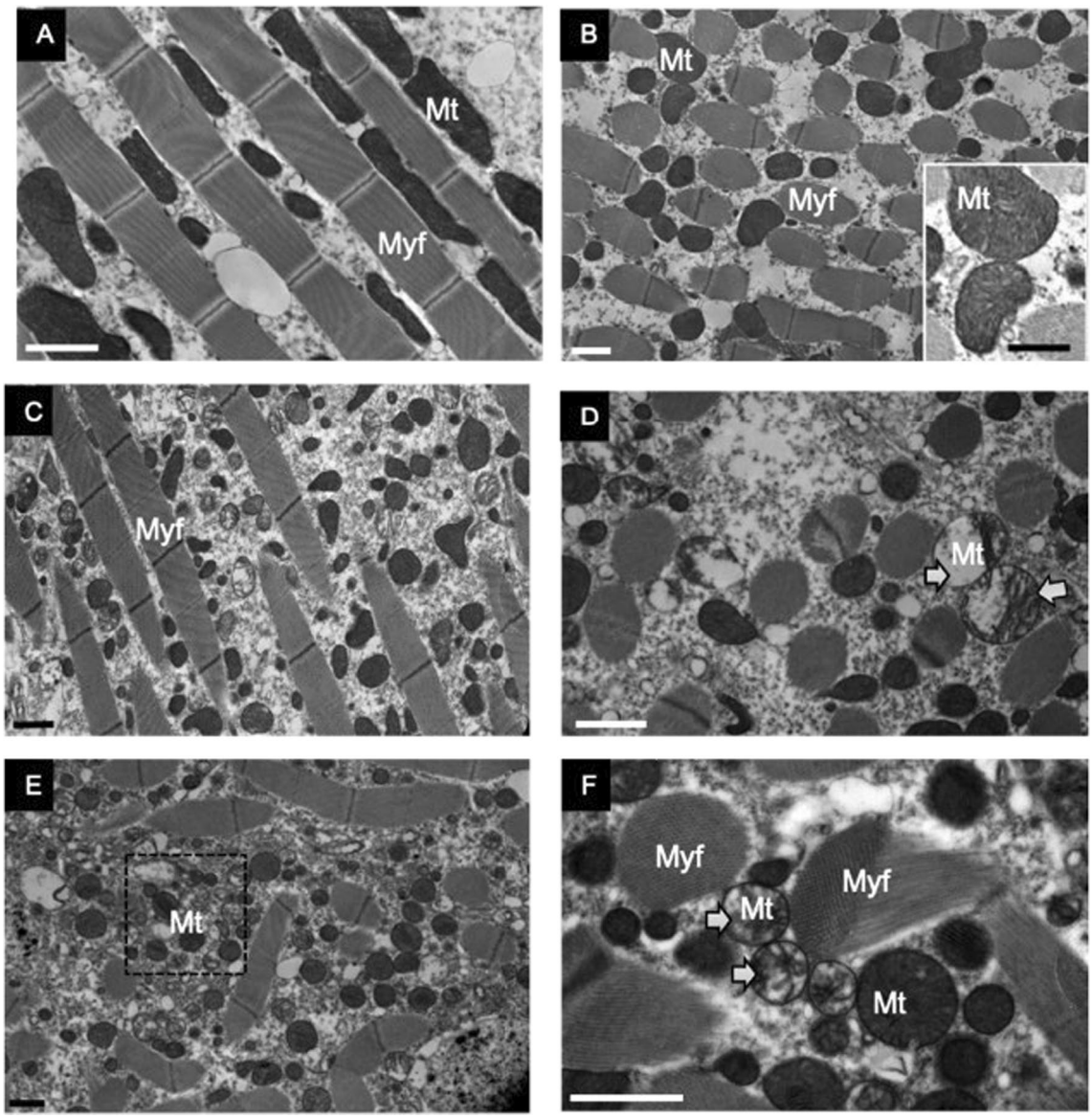

Fig. 6 Transmission electron microscopy (TEM) analysis of indirect flight muscles of *CG14270* knockdown versus normal flies. Representative TEM images of indirect flight muscles (IFM) from wild type (WT) and knockdown *107710kk/+;24B-gal4/+* flies (KDS). **A** Longitudinal and **B** transversal sections of IFM of WT showing normal muscle structure and orientation with normal mitochondrial morphology and cristae ultrastructure (insert in **B**). **C**–**F** IFM of KDS demonstrating swollen mitochondria with extensive vacuolization of the inner membrane (white arrows, **D** and **F**). Note the increase in mitochondrial number (**C** and **E**). Progressing mitochondrial pathology is accompanied by a disturbance in the orientation of the muscle fibers (**E** and **F**); Mt, mitochondria; Myf, myofibril; Scale bars: **A**–**F**, 1 µm, insert 0.5 µm

in the S.S-*TIMM29* participants. This resulted in them having short lifespan, lethargy and severe loss of locomotion activity and climbing abilities that likely reflect severe muscle hypotonia. Moreover, reduced activity of several mitochondrial respiratory chain complexes was demonstrated in dissected muscle preparations (Fig. 7, Xls4- Human Genomics), and ultrastructural analysis of flight muscles revealed abnormal mitochondrial structure mimicking the mitochondrial phenotype seen in S.S- *TIMM29* patients (Fig. 6). These findings demonstrate that the *Drosophila* model recapitulates the human S.S-*TIMM29* participants' phenotype. Interestingly, in a a systematic RNAi-based screen for genes involved in muscle morphogenesis and function in *Drosophila,* the fly AGK ortholog Mulk was identified as one of 78 genes whose knockdown in muscles led to abnormal locomotor behavior [35]. To the best of our knowledge, no

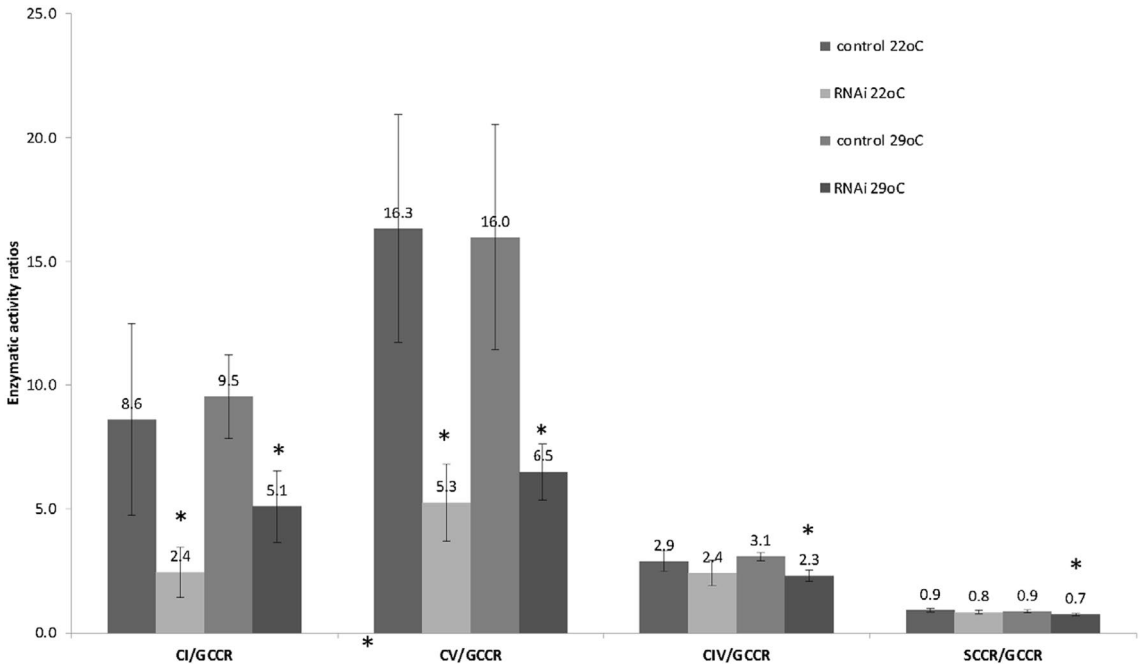

Fig. 7 A significant decrease in the respiratory chain enzymatic activities in the RNAi treated flies compared to the control group. There is a significant decrease of the respiratory chain enzymatic activities in the RNAi treated flies compared to the control group. We calculated the respiratory chain enzymatic activities assayed by spectrophotometry in muscle homogenates from flies grown at different temperatures (22 °C and 29 °C) and ratios to glycerol 3-phosophate dehydrogenase (GCCR) (*$p < 0.05$)

biochemical or ultrastructural phenotypic data related to Mulk is available.

Delving into the clinical and biochemical features of both S.S-*AGK* and S.S-*TIMM29* highlights additional clinical findings which allow us to expand the phenotype of S.S.

Cardiac arrythmia: One S.S-*TIMM29* participant (VII-11) died at home suddenly. We assume that cardiac arrythmia was the cause of his "sudden death" although he did not display cardiomyopathy. Arrythmia was suggested to be the underlying cause of "sudden death" in one S.S-*AGK* patient who did not feature previous cardiac decompensation at the age of 2 years [11]. Interestingly, the *ANT1* homozygous mutant mice model, also featured cardiac arrhythmia [36].

In the S.S-*AGK* participants, motor developmental delay, hypotonia, hyporeflexia, and impaired physical mobility were commonly attributed to muscular weakness due to the mitochondrial myopathy. However, these symptoms could express also neurological abnormalities secondary to central-nervous-system (CNS) involvement. Long-term follow-up of the S.S-*AGK* participants revealed several developmental challenges, such as intellectual disability, psychomotor delay and language acquisition delay or absence [5, 11]. In three S.S-*TIMM29* participants (VI-20, VII-4 & VII-5), we suspected developmental delay due to brain involvement. These three S.S-*TIMM29* participants did not achieve any developmental milestone, nor social eye contact. Also, two of them had elevated level of lactate in their CSF, suggesting mitochondrial encephalopathy. Brain imaging in participant VII-5 revealed periventricular leukomalacia, partial agenesis of corpus callosum and vermis hypoplasia depicted by brain ultrasound and CT scan, respectively. Neuro-radiological examinations were performed in only 30% of the reported S.S-*AGK* cases. This is probably because most of them died within the first or second year of their life and they were assumed to have developmental delay, due to the mitochondrial myopathy [4, 7, 43]. The most common neuroradiological manifestations in the S.S-*AGK* participants include hypoplasia of the brainstem and inferior cerebellar vermis, impaired myelination of the cerebral hemispheres, and brainstem, and cortical infarctions. However, these infarctions follow a vascular pattern different from typical metabolic strokes, which do not adhere to any specific arterial distributions [10]. The developmental delay, neuroradiological findings and elevated CSF lactate in the S.S participants suggest that both S.S types can be described as mitochondrial Encephalo-Cardio-Myopathies. In order to substantiate this possibility, brain MRI and MRS should be added routinely to the study of S.S patients.

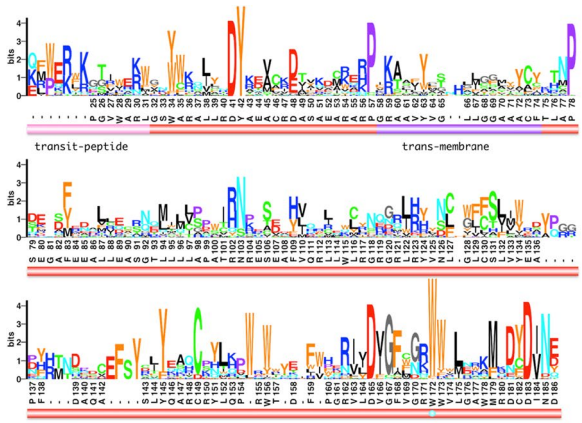

a

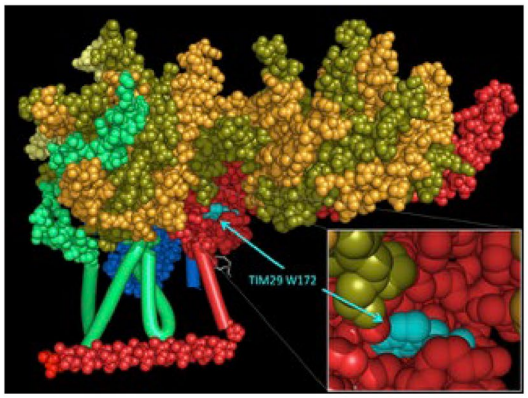

b

Fig. 8 a. Sequence conservation of Tim29 proteins. Sequence logo of the Tim29 protein family (pfam PF10171) uniprot sequence multiple-sequence alignment, with 1010 proteins, spanning chordates, arthropods, nematodes, mollusks, plathyhelminthes, rotifers, and cnidaria (https://www.ebi.ac.uk/interpro/entry/pfam/PF10171/). The height of each column relates to its conservation. The sequences were position-base weighted [https://doi.org/10.1016/0022–2836(94)90032-9]. The total conservation in each column is its relative entropy (Kullback–Leibler distance) using the amino-acids background frequencies in the SwissProt database, with small-sample correction [https://doi.org/10.1038/nbt0406-423]. The amino acid fractions in each column are relative to their weighted odds ratios, as previously described [https://doi.org/10.1016/0378–1119(95)00486-p]. Each column is labeled beneath by its position and residue in human Tim29 protein, with gaps indicating insertion in the alignment relative to the human protein, and the protein transit-peptide and trans-membrane regions, and Trp172 residue are marked. **b** Position of Tim29 W172 in the cryo-structure of human TIM22 complex [doi.org/10.1038/s41422-020–00400-w]. Subunit colors are: TIM22 in light green, AGK in light blue, Tim29 in red with Trp172 in cyan, Tim9 chains in orange, Tim10a chains in olive, and Tim10b in light yellow. The atoms of the proteins aa are shown as spheres, except for the trans-membrane regions that are shown as cylinders. The phosphoethanolamine phospholipid is shown in gray. Inset shows a zoomed view of Tim29 Trp172. Figure made with the PyMol program (https://pymol.org)

The most striking biochemical difference between S.S-*TIMM29* and S.S-*AGK* patients was the constant finding of elevated levels of serum creatine phosphokinase (CK) (HyperCPkemia) in S.S-*TIMM29*, which could progress to rhabdomyolysis (Table 1) [44, 45]. HyperCPKemia has not been reported in S.S-*AGK* patients, except for one recently reported S.S-*AGK* patient [12]. CK, both the mitochondrial CK and the cytosolic CK isoenzymes, play a critical role in the buffering of energy to maintain cellular energy homeostasis [46, 47]. Thus, the hyperCPKemia found in S.S-*TIMM29* patients could denote a central role of Tim29 in the CK metabolism. Many mitochondrial DNA (mtDNA) and nuclear DNA (nDNA) variants cause mitochondrial cytopathies, but only sporadic cases have been reported to be associated with rhabdomyolysis [45]. Thus, the role of Tim29 deficiency in the causation of rhabdomyolysis remains to be elucidated.

The phenotypic resemblance of the S.S-*TIMM29* studied cohort to the adenine nucleotide translocator 1 (*ANT1*) deficient mice model was astonishing two decades ago. Both shared the hypertrophic cardiomyopathy, elevated serum lactate and strikingly abnormal mitochondrial structure in skeletal and cardiac muscle (Fig. 2) [10, 23, 36]. *ANT1* deficiency was demonstrated also in skeletal and cardiac muscles tissues derived from S.S-*AGK* [13, 23] and in a patient with compound heterozygous variants in the *TIMM22* gene [24].

For many years, ANT1, encoded by the *SLC25A4 gene*, was known for its canonical function of forming a channel which moves ADP into ATP out of the mitochondrion to be used as energy source of the cell. However, over the years, ANT1 has been shown to be a moonlighting protein, a biological phenomenon in which a protein with a canonical function can acquire additional roles during evolution [48]. In addition to its canonical function, ANT1 was shown to drive mitophagy, independent of the nucleotide exchange [36]. Thus, the profound abnormal mitochondrial changes shown in the *ANT1* mice model [35], in previously reported S.S-*AGK* tissues [10, 23], and in skeletal and cardiac muscle tissues derived from the S.S-*TIMM29* cohort (Fig. 2a,b c and c), could be attributed to the blunted mitophagy associated with *ANT1* deficiency [49]. ANT1 was also shown to be involved in the assembly of the respiratory chain complexes (RCC), a function which could be involved in the multiple mitochondrial respiratory chain complexes (MMRCC) deficiency depicted in the S.S patients (see below) [50, 51]. Recently, variants in the *ANT1* were shown to be associated with clogging of cytosolic synthesized proteins targeted to the inner-mitochondrial membrane at the translocase of the outer membrane (TOM) complex [52]**.** Tim29 was shown to connect between the inner

mitochondrial membrane and TOM complex [19, 22]. Combining these facts thus lead us to hypothesize that Tim29 deficiency may also affect indirectly protein transport from the cytosol into the mitochondria. This hypothesis needs to be addressed in future studies.

Multiple Mitochondrial Respiratory Chain Complexes (MMRCC) deficiency has been reported in ~ 49% of patients with mitochondrial disorders [53]. Combined defects of complexes I, III, IV and V in various combinations could be due to variants in genes that encode enzymes of mtDNA replication machinery, or maintain a balanced mitochondrial nucleotide pool or genes encoding proteins involved in mitochondrial fusion [54]. While most of the studied S.S-*TIMM29* participants showed MMRCC deficiency in various combinations (Table 2), it was not constantly reported in the S.S-AGK participants [4–6, 12]**.**This difference should be further explored.

The pyruvate dehydrogenase complex (PDHc) catalyzes the irreversible decarboxylation of pyruvate into acetyl-CoA. PDHc deficiency demonstrated in most of the S.S-*TIMM29* studied participants (Table 2) was previously reported in only two S.S-*AGK* cases [23]. The resulting phenotype of PDHc deficiency mainly affects the central nervous system [55]. This raises the hypothesis that PDHc deficiency could contribute to the neurological symptoms and brain malformation in S.S individuals.

Recently, mitochondrial pyruvate carriers MPC1 and MPC2 were shown to constitute novel substrates of TIM22 in yeasts and humans [56]. The MPCs reside at a central metabolic point by transporting cytosolic pyruvate across the inner mitochondrial membrane (IMM), thereby linking glycolysis with oxidative phosphorylation [57, 58]. Thus, MPCs deficiencies could be involved in causing PDHc deficiency in S.S. However, it cannot explain the difference in the frequency of PDHc deficiency in S.S-*TIMM29* compared to S.S-*AGK* individuals. Interestingly, individuals with MPC1 and MPC2 deficiency feature mainly neurological abnormalities [57, 58]. Thus, MPCs deficiency can be added to the list of factors which could contribute to the abnormal neurological phenotype depicted in some of the S.S participants. We still do not know if the difference in the frequency of PDHc deficiency in the two S.S types uncovers a specific, not yet defined function**,** whereby Tim29 differs from AGK. It also remains unclear the extent to which the biochemical differences between S.S-*TIMM29* and S.S-*AGK* individuals uncover novel specific functions of Tim29.

Conclusion

In summary, we report a novel form of S.S caused by *a* biallelic variant *in TIMM29*. Its phenotype resembles to large extent the severe infantile fatal form of S.S caused by biallelic variants in the *AGK* (S.S-*AGK*). Nevertheless, the present study uncovers several biochemical differences between the two S.S types, including the hyper-CPKemia being almost unique for S.S-*TIMM29* cohort, the different frequency of MMRCC and PDHc deficiencies among the two S.S types. We propose to designate the S.S associated with *TIMM29* homozygous variant as S.S-*TIMM29*. The precise molecular pathomechanism underlying these differences is yet to be elucidated.

Supplementary Information

The online version contains supplementary material available at https://doi.org/10.1186/s40246-025-00723-y.

Additional file1
Additional file2
Additional file3
Additional file4
Additional file5
Additional file6
Additional file7
Additional file8
Additional file9
Additional file10
Additional file11

Acknowledgements
The authors particularly thank all the study participants and their parents for participating in this research. We gratefully acknowledge the collaboration of physicians who sent us DNA samples of their Sengers' patients prior to the determination of the biallelic AGK variants as the cause of the Sengers syndrome in their patients (2012-2013).

Author contribution
CRediT statements Term Definition Conceptualization Adel Shalata and Hanna Mandel, Methodology Development or design of methodology; Adel Shalata; creation of models, Ronen Spiegel, Euvgeni Vlodavsky, Pierre Rustin, Irena Manov, Galit Tal Software Adel Shalata, Mohammed Mahroum, Shmuel Pietrokovsk, Dan Gieger, Chaya Furman, Validation Adel Shalata, Mohammed Mahroum, Ann Saada, Yarin Hadid, Robert Desnick Formal analysis Adel Shalata, Ann Saada, Hanna Mandel, Adi Salzberg, Avraham Lorber Investigation Adel Shalata, Hanna Mandel, Adi Salzberg, Asaad Khoury Resources Adel Shalata and Hanna Mandel. Data Curation Adel Shalata, Hanna Mandel and Adi Salzberg, Adnan Higazi, Writing—Original Draft Adel Shalata and Hanna Mandel. Writing—Review & Editing All authors Visualization Adel Shalata, Ann Saada, Hanna Mandel, Adi Salzberg, Mohammed Mahroum, Zaher Eldin Shalata, Yarin Hadid, Avraham Shaag Supervision Adel Shalata and Hanna Mandel. Project administration Adel Shalata and Hanna Mandel, Varda Barash Funding acquisition Adel Shalata, Hanna Mandel and Adi Salzberg.

Funding
This study was financed by a grant of 100,000 INS (HM & AS) from the Chief Scientist Ministry of Health for "Homozygosity mapping of the Sengers Syndrome gene (hypertrophic cardiomyopathy, cataract and lactic acidosis". The authors would also like to thank Ginatuna Association for NGS funding.

Availability of data and materials
The datasets used to support the findings of this study have been made available.

Declarations

Competing interests
The authors declare no competing interests.

Author details
[1]Bnai Zion Medical Center, The Simon Winter Institute for Human Genetics, Haifa, Israel. [2]Seba Rihana Medical Center, Sakhnin, Israel. [3]Ruth and Bruce Rappaport Faculty of Medicine, Technion-Israel Institute of Technology, Haifa, Israel. [4]Department of Genetics, Hadassah Medical Center, Jerusalem, Israel. [5]Faculty of Medicine, Hebrew University of Jerusalem, Jerusalem, Israel. [6]Department of Medical Laboratory Sciences, Hadassah Academic College, Jerusalem, Israel. [7]Department of Genetics and Genomic Sciences, Icahn School of Medicine at Mount Sinai, New York, NY, USA. [8]Department of Pediatric Cardiology, Rambam Medical Center, Haifa, Israel. [9]Clalit Health Care, Haifa, Israel. [10]Monique and Jacques Roboh Department of Genetic Research, Hadassah-Hebrew University Medical Center, Jerusalem, Israel. [11]Department of Biochemistry, Hadassah-Hebrew University Medical Center, Jerusalem, Israel. [12]Department of Pediatric B, Emek Medical Center, Afula, Israel. [13]Department of Pathology, Rambam Health Care Campus, Haifa, Israel. [14]NeuroDiderot, Inserm Université Paris Cité, 75019 Paris, France. [15]Department of Molecular Genetics, Weizmann Institute of Science, 7610001 Rehovot, Israel. [16]Institute of Evolution, University of Haifa, Haifa, Israel. [17]Computer Science Department, Technion, Israel Institute of Technology, Haifa, Israel. [18]The Unit for Metabolic Disorders, Rambam Medical Center, Haifa, Israel. [19]Department of Genetics and Metabolic Disorders, Ziv Medical Center, Safed, Israel.

Received: 1 November 2024 Accepted: 3 February 2025
Published: 28 February 2025

References
1. Sengers RC, Trijbels JM, Willems JL, Daniels O, Stadhouders AM. Congenital cataract and mitochondrial myopathy of skeletal and heart muscleassociated with lactic acidosis after exercise. J Pediatr. 1975;86(6):873–80. https://doi.org/10.1016/s0022-3476(75)80217-4.
2. Smeitink JA, Sengers RC, Trijbels JM, et al. Fatal neonatal cardiomyopathy associated with cataract and mitochondrialmyopathy. Eur J Pediatr. 1989;148(7):656–9. https://doi.org/10.1007/BF00441527.
3. van Ekeren GJ, Stadhouders AM, Smeitink JA, Sengers RC. A retrospective study of patients with the hereditary syndrome of congenitalcataract, mitochondrial myopathy of heart and skeletal muscle and lactic acidosis. Eur J Pediatr. 1993;152(3):255–9. https://doi.org/10.1007/BF01956157.
4. Mayr JA, Haack TB, Graf E, et al. Lack of the mitochondrial protein acylglycerol kinase causes Sengers syndrome. Am J Hum Genet. 2012;90(2):314–20. https://doi.org/10.1016/j.ajhg.2011.12.005.
5. Haghighi A, Haack TB, Atiq M, et al. Sengers syndrome: six novel AGK mutations in seven new families and review of thephenotypic and mutational spectrum of 29 patients. Orphanet J Rare Dis. 2014;9:119. https://doi.org/10.1186/s13023-014-0119-3.
6. Wang B, Du Z, Shan G, Yan C, Zhang VW, Li Z. Case report: two Chinese infants of sengers syndrome caused by mutations in AGKGene. Front Pediatr. 2021;9:639687. https://doi.org/10.3389/fped.2021.639687.
7. Panicucci C, Schiaffino MC, Nesti C, et al. Long term follow-up in two siblings with Sengers syndrome: case report. Ital J Pediatr. 2022;48(1):180. https://doi.org/10.1186/s13052-022-01370-y.
8. Aldahmesh MA, Khan AO, Mohamed JY, Alghamdi MH, Alkuraya FS. Identification of a truncation mutation of acylglycerol kinase (AGK) gene in anovel autosomal recessive cataract locus. Hum Mutat. 2012;33(6):960–2. https://doi.org/10.1002/humu.22071.
9. Calvo SE, Compton AG, Hershman SG, et al. Molecular diagnosis of infantile mitochondrial disease with targetednext-generation sequencing. Sci Transl Med. 2012;4(118):118ra10. https://doi.org/10.1126/scitranslmed.3003310.
10. Siriwardena K, Mackay N, Levandovskiy V, et al. Mitochondrial citrate synthase crystals: novel finding in Sengers syndrome causedby acylglycerol kinase (AGK) mutations. Mol Genet Metab. 2013;108(1):40–50. https://doi.org/10.1016/j.ymgme.2012.11.282.
11. Allali S, Dorboz I, Samaan S, et al. Mutation in the AGK gene in two siblings with unusual Sengers syndrome. Metab Brain Dis. 2017;32(6):2149–54. https://doi.org/10.1007/s11011-017-0101-6.
12. Guleray N, Kosukcu C, Taskiran ZE, et al. Atypical presentation of Sengers syndrome: a novel mutation revealed withpostmortem genetic testing. Fetal PediatrPathol. 2020;39(2):163–71. https://doi.org/10.1080/15513815.2019.1639089.
13. Jordens EZ, Palmieri L, Huizing M, et al. Adenine nucleotide translocator 1 deficiency associated with Sengers syndrome. Ann Neurol. 2002;52(1):95–9. https://doi.org/10.1002/ana.10214.
14. Morava E, Hogeveen M, De Vries M, Ruitenbeek W, de Boode WP, Smeitink J. Normal serum alanine concentration differentiates transient neonatal lacticacidemia from an inborn error of energy metabolism. Biol Neonate. 2006;90(3):207–9. https://doi.org/10.1159/000093590.
15. Rath S, Sharma R, Gupta R, et al. MitoCarta3.0: an updated mitochondrial proteome now with sub-organellelocalization and pathway annotations. Nucl Acids Res. 2021;49(D1):D1541–7. https://doi.org/10.1093/nar/gkaa1011.
16. Wiedemann N, Pfanner N. Mitochondrial machineries for protein import and assembly. Annu Rev Biochem. 2017;86:685–714. https://doi.org/10.1146/annurev-biochem-060815-014352.
17. Neupert W, Herrmann JM. Translocation of proteins into mitochondria. Annu Rev Biochem. 2007;76:723–49. https://doi.org/10.1146/annurev.biochem.76.052705.163409.
18. Mokranjac D, Neupert W. The many faces of the mitochondrial TIM23 complex. BiochimBiophys Acta. 2010;1797(6–7):1045–54. https://doi.org/10.1016/j.bbabio.2010.01.026.
19. Kang Y, Baker MJ, Liem M, et al. Tim29 is a novel subunit of the human TIM22 translocase and is involved incomplex assembly and stability. Elife. 2016. https://doi.org/10.7554/eLife.17463.
20. Palmer CS, Anderson AJ, Stojanovski D. Mitochondrial protein import dysfunction: mitochondrial disease, neurodegenerative disease and cancer. FEBS Lett. 2021;595(8):1107–31. https://doi.org/10.1002/1873-3468.14022.
21. Vukotic M, Nolte H, König T, et al. Acylglycerol kinase mutated in sengers syndrome is a subunit of the TIM22 proteintranslocase in mitochondria. Mol Cell. 2017;67(3):471-483.e7. https://doi.org/10.1016/j.molcel.2017.06.013.
22. Qi L, Wang Q, Guan Z, et al. Cryo-EM structure of the human mitochondrial translocase TIM22 complex. Cell Res. 2021;31(3):369–72. https://doi.org/10.1038/s41422-020-00400-w.
23. Morava E, Sengers R, Ter Laak H, et al. Congenital hypertrophic cardiomyopathy, cataract, mitochondrial myopathy anddefective oxidative phosphorylation in two siblings with Sengers-like syndrome. Eur J Pediatr. 2004;163(8):467–71. https://doi.org/10.1007/s00431-004-1465-2.
24. Pacheu-Grau D, Callegari S, Emperador S, et al. Mutations of the mitochondrial carrier translocase channel subunit TIM22 causeearly-onset mitochondrial myopathy. Hum Mol Genet. 2018;27(23):4135–44. https://doi.org/10.1093/hmg/ddy305.
25. Pfanner N, Warscheid B, Wiedemann N. Mitochondrial proteins: from biogenesis to functional networks. Nat Rev Mol Cell Biol. 2019;20(5):267–84. https://doi.org/10.1038/s41580-018-0092-0.
26. Callegari S, Richter F, Chojnacka K, et al. TIM29 is a subunit of the human carrier translocase required for proteintransport. FEBS Lett. 2016;590(23):4147–58. https://doi.org/10.1002/1873-3468.12450.
27. Kang Y, Stroud DA, Baker MJ, et al. Sengers syndrome-associated mitochondrial acylglycerol kinase is a subunit of thehuman TIM22 protein import complex. Mol Cell. 2017;67(3):457-470.e5. https://doi.org/10.1016/j.molcel.2017.06.014.
28. Saada A, Bar-Meir M, Belaiche C, Miller C, Elpeleg O. Evaluation of enzymatic assays and compounds affecting ATP production inmitochondrial respiratory chain complex I deficiency. Anal Biochem. 2004;335(1):66–72. https://doi.org/10.1016/j.ab.2004.08.015.
29. Reisch AS, Elpeleg O. Biochemical assays for mitochondrial activity: assays of TCA cycle enzymes andPDHc. Methods Cell Biol. 2007;80:199–222. https://doi.org/10.1016/S0091-679X(06)80010-5.
30. Chretien D, Rustin P. Mitochondrial oxidative phosphorylation: pitfalls and tips in measuring andinterpreting enzyme activities. J Inherit Metab Dis. 2003;26(2–3):189–98. https://doi.org/10.1023/a:1024437201166.
31. Bénit P, Goncalves S, Philippe Dassa E, Brière JJ, Martin G, Rustin P. Three spectrophotometric assays for the measurement of the five respiratory

chaincomplexes in minuscule biological samples. Clin Chim Acta. 2006;374(1–2):81–6. https://doi.org/10.1016/j.cca.2006.05.034.
32. Manis T, George-Varghese B, Kashani J. Rhabdomyolysis—go big or go home. Am J Emerg Med. 2019;37(12):2194–6. https://doi.org/10.1016/j.ajem.2019.03.024.
33. Wortmann SB, Duran M, Anikster Y, et al. Inborn errors of metabolism with 3-methylglutaconic aciduria as discriminativefeature: proper classification and nomenclature. J Inherit Metab Dis. 2013;36(6):923–8. https://doi.org/10.1007/s10545-012-9580-0.
34. Vincent AE, Ng YS, White K, et al. The spectrum of mitochondrial ultrastructural defects in mitochondrial myopathy. Sci Rep. 2016;6:30610. https://doi.org/10.1038/srep30610.
35. Schnorrer F, Schönbauer C, Langer CC, Dietzl G, Novatchkova M, Schernhuber K, Fellner M, Azaryan A, Radolf M, Stark A, Keleman K, Dickson BJ. Systematic genetic analysis of muscle morphogenesis and function in *Drosophila*. Nature. 2010;464(7286):287–91. https://doi.org/10.1038/nature08799.
36. Graham BH, Waymire KG, Cottrell B, Trounce IA, MacGregor GR, Wallace DC. A mouse model for mitochondrial myopathy and cardiomyopathy resulting from adeficiency in the heart/muscle isoform of the adenine nucleotide translocator. Nat Genet. 1997;16(3):226–34. https://doi.org/10.1038/ng0797-226.
37. Carmi R, Rokhlina T, Kwitek-Black AE, et al. Use of a DNA pooling strategy to identify a human obesity syndrome locus onchromosome 15. Hum Mol Genet. 1995;4(1):9–13. https://doi.org/10.1093/hmg/4.1.9.
38. Arbour NC, Zlotogora J, Knowlton RG, et al. Homozygosity mapping of achromatopsia to chromosome 2 using DNA pooling. Hum Mol Genet. 1997;6(5):689–94. https://doi.org/10.1093/hmg/6.5.689.
39. Silberstein M, Tzemach A, Dovgolevsky N, Fishelson M, Schuster A, Geiger D. Online system for faster multipoint linkage analysis via parallel execution on thousands of personal computers. Am J Human Genet. 2006;78(6):922–35. https://doi.org/10.1086/504158.
40. Gramates LS, Marygold SJ, Dos SG, et al. FlyBase at 25: looking to the future. Nucleic Acids Res. 2017;45(D1):D663–71. https://doi.org/10.1093/nar/gkw1016.
41. Dietzl G, Chen D, Schnorrer F, et al. A genome-wide transgenic RNAi library for conditional gene inactivation in *Drosophila*. Nature. 2007;448:151–6.
42. Ni J, Zhu Z, Wang G, Shen Y, Zhang Y, Wu P. Intragenic suppressor of Osiaa23 revealed a conserved tryptophan residue crucial for protein-protein interactions. PLoS ONE. 2014;9(1):e85358. https://doi.org/10.1371/journal.pone.0085358.PMID:24454849;PMCID:PMC3893212.
43. Perry MS, Sladky JT. Neuroradiologic findings in Sengers syndrome. Pediatr Neurol. 2008;39(2):113–5. https://doi.org/10.1016/j.pediatrneurol.2008.05.003.
44. Yazıcı H, KalkanUçar S. A metabolism perspective on pediatric rhabdomyolysis. Trends Pediatr. 2021;2(4):147–53. https://doi.org/10.4274/TP.galenos.2021.30502.
45. Rawson ES, Clarkson PM, Tarnopolsky MA. Perspectives on Exertional Rhabdomyolysis. Sports Med. 2017;47(Suppl 1):33–49. https://doi.org/10.1007/s40279-017-0689-z.
46. Schlattner U, Tokarska-Schlattner M, Wallimann T. Mitochondrial creatine kinase in human health and disease. BiochimBiophys Acta. 2006;1762(2):164–80. https://doi.org/10.1016/j.bbadis.2005.09.004.
47. Schlattner U, Kay L, Tokarska-Schlattner M. Mitochondrial proteolipid complexes of creatine kinase. SubcellBiochem. 2018;87:365–408. https://doi.org/10.1007/978-981-10-7757-9_13.
48. Houten SM. Protein moonlighting in inborn errors of metabolism: the case of themitochondrial acylglycerol kinase. J Inherit Metab Dis. 2017;40(6):755–6. https://doi.org/10.1007/s10545-017-0090-y.
49. Hoshino A, Wang WJ, Wada S, et al. The ADP/ATP translocase drives mitophagy independent of nucleotide exchange. Nature. 2019;575(7782):375–9. https://doi.org/10.1038/s41586-019-1667-4.
50. Lu YW, Acoba MG, Selvaraju K, et al. Human adenine nucleotide translocases physically and functionally interact withrespirasomes. Mol Biol Cell. 2017;28(11):1489–506. https://doi.org/10.1091/mbc.E17-03-0195.
51. Parodi-Rullán RM, Chapa-Dubocq X, Guzmán-Hernández R, et al. The role of adenine nucleotide translocase in the assembly of respiratory supercomplexes in cardiac cells. Cells. 2019;8(10):1247. https://doi.org/10.3390/cells8101247.
52. Coyne LP, Wang X, Song J, et al. Mitochondrial protein import clogging as a mechanism of disease. Elife. 2023. https://doi.org/10.7554/eLife.84330.
53. Mayr JA, Haack TB, Freisinger P, et al. Spectrum of combined respiratory chain defects. J Inherit Metab Dis. 2015;38(4):629–40. https://doi.org/10.1007/s10545-015-9831-y.
54. El-Hattab AW, Craigen WJ, Scaglia F. Mitochondrial DNA maintenance defects. BiochimBiophys Acta Mol Basis Dis. 2017;1863(6):1539–55. https://doi.org/10.1016/j.bbadis.2017.02.017.
55. Pavlu-Pereira H, Silva MJ, Florindo C, et al. Pyruvate dehydrogenase complex deficiency: updating the clinical, metabolic andmutational landscapes in a cohort of Portuguese patients. Orphanet J Rare Dis. 2020;15(1):298. https://doi.org/10.1186/s13023-020-01586-3.
56. Gomkale R, Cruz-Zaragoza LD, Suppanz I, et al. Defining the substrate spectrum of the TIM22 complex identifies pyruvate carriersubunits as unconventional cargos. Curr Biol. 2020;30(6):1119-1127.e5. https://doi.org/10.1016/j.cub.2020.01.024.
57. Jiang H, Alahmad A, Fu S, et al. Identification and characterization of novel MPC1 gene variants causing mitochondrial pyruvate carrier deficiency. J Inherit Metab Dis. 2022;45(2):264–77. https://doi.org/10.1002/jimd.12462.
58. Yiew NKH, Finck BN. The mitochondrial pyruvate carrier at the crossroads of intermediary metabolism. Am J Physiol Endocrinol Metab. 2022;323(1):E33–52. https://doi.org/10.1152/ajpendo.00074.2022.

Publisher's Note